High-Throughput Surface Preparation for Flexible Slot Die Coated Perovskite Solar Cells

Mikas Remeika[a], Luis K. Ono[a], Maki Maeda[a], Zhanhao Hu[a], Yabing Qi[a]*

[a]Energy Materials and Surface Sciences Unit (EMSS), Okinawa Institute of Science and Technology Graduate University (OIST), 1919-1 Tancha, Onna-son, Okinawa, Japan.

*Corresponding author: Yabing.Qi@OIST.jp

Abstract

To achieve industrially viable fabrication process for perovskite-based solar cells, every process step must be optimized for maximum throughput. We present a study of substituting laboratory-type UV-Ozone surface treatment with a high-throughput Corona treatment in a scalable perovskite solar cell fabrication process. It is observed that water contact angle measurements provide insufficient information to determine the necessary dose of Corona or UV-Ozone treatment, but the surface carbon signal measured by x-ray photoelectron spectroscopy accurately identifies when surface contamination has been completely removed. Furthermore, we observe highly accelerated de-contamination of ZnO surfaces by UV-Ozone treatment. The effect can be explained by photocatalytic O_2^- ion generation indicating that UV-Ozone treatment is also applicable in high-throughput processing.

1 Introduction

Perovskite solar cell power conversion efficiency has advanced at an unprecedented rate (up to 22.1% [1]) and is now competitive with many commercialized technologies such as CIGS (22.6% [1]) and CdTe (22.1% [1]). Solution processing is promising to lead to ultra-low-cost manufacturing, but commonly employed laboratory methods (e.g. spin coating) cannot be scaled to meet industrial production requirements. As a result, many laboratories are beginning to work with scalable fabrication methods such as slot-die coating ([2-8]) and ultrasonic spray coating ([9-15]) to ensure that advances in performance can be rapidly transferred to industrial production. Transitioning from spin-coating to scalable fabrication, researchers often discover that many aspects that could be considered negligible in small scale fabrication become important for scalable fabrication technologies.

Substrate surface preparation is a key aspect of fabrication that achieves high production yields. Contamination that is not eliminated during substrate preparation may affect every layer of the device. Furthermore, uniform surface condition over a large area is a prerequisite for uniform solution coating. Rapid processing is also a requirement because long process time impacts fabrication cost.

In this article we discuss an implementation of Corona treatment as a scalable substitute for UV-Ozone treatment. UV-Ozone treatment is frequently employed in research laboratories to remove surface contamination and increase surface energy of substrates (improve wettability) e.g., see [16, 17]. It is a reliable technique, however, typical exposure times of 5-15 min make it poorly compatible with rapid processing. Corona treatment is a rapid technique (sub-second treatment times) that is widely applied in industry (e.g., for printing on plastic films) and is compatible with roll-to-roll processing. We present a study of substituting UV-Ozone treatment with Corona treatment in a slot-die coating process for perovskite solar cells and discuss some considerations that need to be taken into account when designing a surface treatment process.

2 Materials and Methods

Device fabrication was accomplished as follows. Flexible PET film with pre-patterned ITO coating was cleaned by high pressure air flow to remove surface particles, treated by adhesive roller (Teknek DCR Hand Roller) to remove microscopic particles, and decontaminated with UV-Ozone (15 min) or Corona (1000 Ws/m^2) treatment. Electron selective layer was deposited by slot-die coating of ZnO nanoparticle suspension (Nanograde N-10, 2.5% by weight in isopropanol (IPA), particle size 10-15 nm), with a substrate speed of 0.6 cm/s, an ink pump rate 60 of µL/min, and the substrate temperature of 70 °C. After coating, the substrate was heated to 100 °C (in air), annealed for 2 hours, then allowed to cool to room temperature. PbI_2 precursor layer was deposited by slot-die coating solution of 0.47 mg/mL PbI_2 (Sigma Aldrich) in DMSO (substrate speed 0.6 cm/s, temperature 70 °C, ink pump rate 20 µL/min. N_2 flow was applied to accelerate evaporation of dimethyl sulfoxide during PbI_2 coating (see section 3.1). $MAPbI_3$ layer was completed by slot-die application of the MAI ink (20 mg/mL in dehydrated IPA, substrate speed 0.6 cm/s, temperature 70 °C, pump rate 70 µL/min, repeated 3 times). Hole selective layer was deposited by slot-die application of a P3HT-based ink (20mg P3HT, 7 µL Li-TFSI dopant (27 mg/mL Li-TFSI in Acetonitrile), 3.5 µL 4-terp-butylpiridine, 1 mL O-Dichlorobenzene, prepared with dehydrated solvents in N_2 glove box), substrate speed 0.6 cm/s, temperature 70 °C, pump rate 45 µL/min, repeated 3 times. Device area of $1cm^2$ was defined by thermal evaporation of an Au electrode (80 nm). In all cases the slot die applicator width was 12 mm. Unless otherwise specified, solvents were regular non-dehydrated grade. Reagents were used as received, without further purification.

UV-Ozone treatment was performed for a specified length of time by a table top UV-Ozone treatment system capable of treating rigid or flexible substrates (Jelight 42A-100). Corona treatment was performed by a Vetaphone CP-Lab corona treatment system designed to process flexible substrates. Corona treatment system was operated at substrate speed of between 4 and 10 m/s.

Electrical characterization of devices was performed by ORIEL Sol1A solar simulator and Keithley 2420 source-measure unit, with dwell time of 100 ms at each measured point. Cross-sectional images were obtained by FIB milling and SEM imaging using FEI Helios G3 dual beam system. Optical microscope images were acquired by a Leica DM4000 B microscope.

The surface electronic properties of ZnO were characterized by XPS (Kratos AXIS ULTRA HAS, monochromated Al-Kα = 1486.6 eV) in order to observe effect of UV-ozone and Corona treatments on the surface chemical compositions. The binding energy (BE) was calibrated by measuring the Fermi edge (E_F = 0 eV) and Au-$4f_{7/2}$ (84.0 eV) on a clean Au surface. Great care was taken in order to mitigate X-ray exposure time when characterizing ZnO samples. X-ray induced sample damage was monitored by taking five

consecutive scans and comparing these spectra. Acquisition time for each scan varied from 20 to 70 s depending on the core level regions. The five scans were averaged to a single spectrum if significant change was not observed. XPS intensities for each chemical component was normalized with respect to the Zn $2p_{3/2}$ signal height at BE of 1022.5 eV.

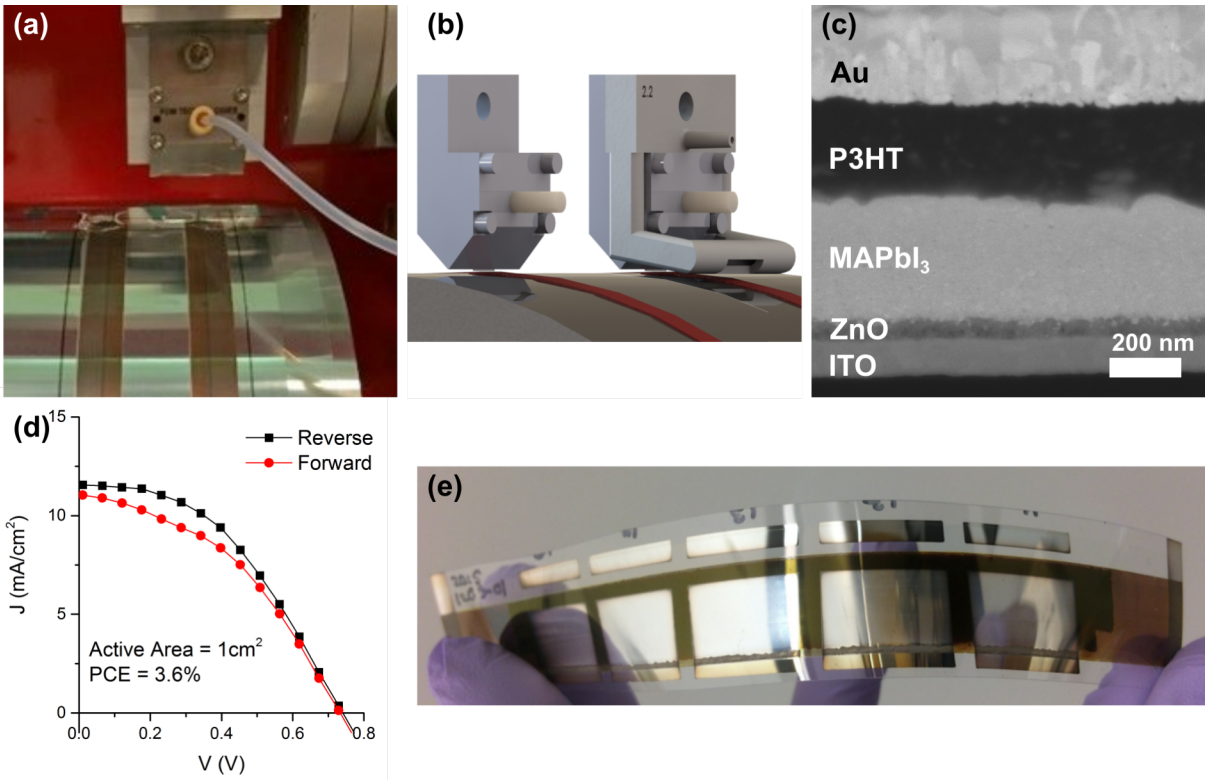

Figure 1. (a) Application of perovskite absorber by slot die coating. Slot die head is shown elevated immediately after coating MAI solution over PbI_2. Red stripes are perovskite strips formed immediately after coating PbI_2 by MAI. (b) Drawing of the slot die head with (right) and without (left) the air flow nozzle used to accelerate drying on PbI_2 immediately after slot die coating (not shown in (a)). (c) SEM cross section image of the slot-die coated perovskite solar cell on a flexible PET substrate. (d) IV characteristic of a top performing device under AM1.5 illumination. Forward and reverse voltage sweeps are shown to demonstrate minimal hysteresis. (e) A strip of flexible solar cells fabricated by slot-die coating. Each device has active area of 1 cm^2.

3 Results and Discussion

3.1 Device Fabrication

To advance scalable fabrication technology for solution processed perovskite solar cells, a table-top slot-die coating system was used to develop a roll-to-roll compatible coating process. Slot-die coating is commonly employed in industry for high-throughput coating, and in recent years laboratory sized machines have become available. Small scale slot-die coating tools allow development of coating processes with only a small investment, and permit a rapid transfer of technology from laboratory to large scale production. Several groups have demonstrated slot-die coating of functional layers for perovskite solar cell fabrication [2-8].

The proof-of-concept process was designed to employ low cost materials, in particular substituting P3HT for a more conventional spiro-MEOTAD, due to lower cost and an established record of reliable large area

coating. We implemented a device structure of polyethylene terephthalate (PET) \ Indium Tin Oxide (ITO) \nanoparticle (np-)ZnO\ $MAPbI_3$ \ doped poly(3-hexylthiophene-2,5-diyl) (P3HT) \ Au with np-ZnO, $MAPbI_3$, and P3HT layers applied by slot-die coating (details of device fabrication can be found in Section 2). UV Ozone / Corona treatment was applied to ITO surface before coating ZnO nanoparticle ink, and to ZnO surface after annealing (before coating PbI_2 precursor to $MAPbI_3$).

Slot die coating was accomplished using a Mini Roll Coater by FOM technologies. Figure 1a shows the roll coating tool immediately after coating MAI ink over PbI_2 precursor. For the purpose of coating the PbI_2 precursor layer the system was modified to add a gas quench system, similar to what was implemented by Hwang et al[3]. Solvent evaporation rate dramatically affects the texture of solution coated PbI_2 films and we found that uniformly translucent films could be achieved if the slot-die coating head was followed immediately by nitrogen nozzle that uniformly applied a strong flow of nitrogen over the wet PbI_2 film. A 3D rendering of the nozzle design mounted on the slot-die head is shown in Figure 1b. The nozzle was fabricated by 3D printing and is specifically designed to apply a uniform laminar flow of gas onto the wet film, while preventing flow of gas toward the slot die head which could disturb application of liquid ink.

The cross-sectional SEM image of the fabricated device is shown in Figure 1c. Maximum power conversion efficiency achieved by such a device is 3.6 % with negligible hysteresis (Figure 1d). Several complete devices are shown in the Figure 1e. The main goal of this work was to study the implementation of high-throughput Corona treatment to perovskite solar cell fabrication; therefore, optimization of slot-die coated device performance will be addressed in future work. The complete devices are presented here as a proof concept, to demonstrate that processing conditions were appropriate for device fabrication.

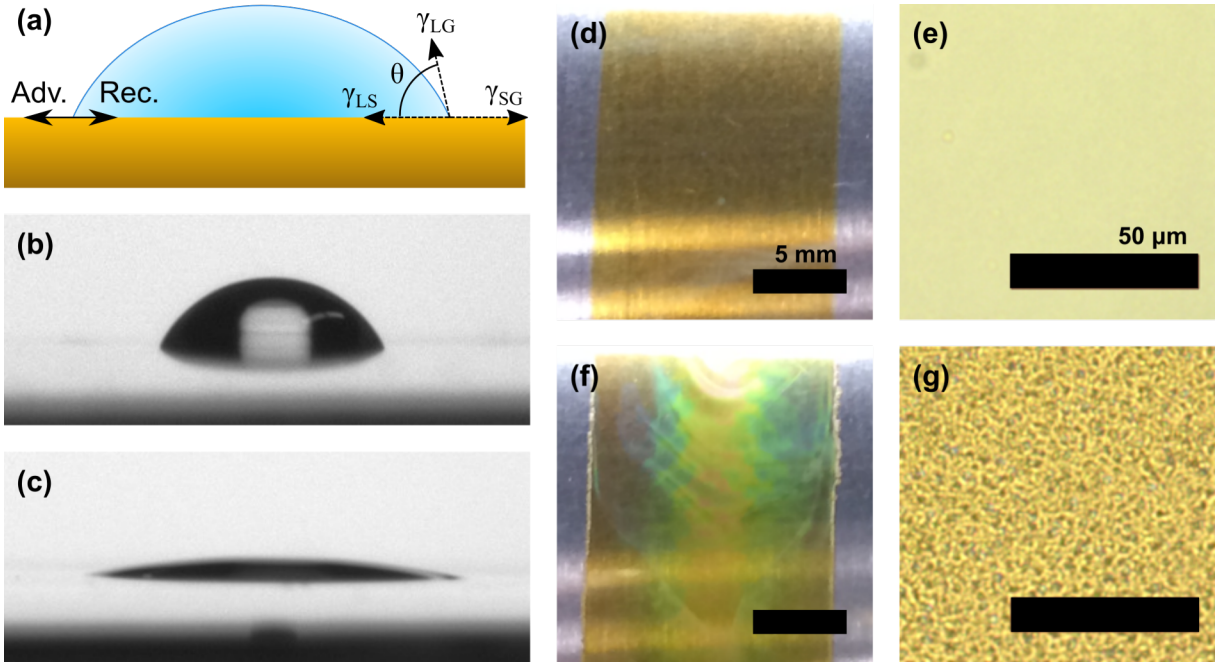

Figure 2 (a) Schematic of a water droplet on a solid surface. γ_{SL}, γ_{LG}, and γ_{SG} are solid-liquid, liquid-gas, and solid gas surface/interface tension forces respectively. When the three forces balance, contact angle of θ is achieved. Left side of the drop indicates directions of advancing and receding liquid edge (see Appendix A). (b) water droplet profile photo on an untreated ITO surface. (c) Water droplet profile photo on a ITO substrate after 15 min UV-Ozone treatment. (d) *Visually smooth PbI_2 texture obtained by coating* ZnO treated with UV-Ozone. (e) *Transmission optical microscope image of smooth PbI_2 obtained by* coating UV-Ozone treated ZnO. (f) *Visually rough texture of PbI_2 obtained by coating insufficiently Corona treated ZnO*, scale bar is the same as (d). (g) *Transmission optical microscope image of PbI_2 obtained by coating insufficiently Corona-treated PbI_2*, scale bar is the same as (e).

3.2 Surface Treatment

Three types of surface treatments by reactive oxygen are common in research laboratories: UV-Ozone, Corona, and Oxygen Plasma. See Appendix B for a detailed discussion. While all three treatments achieve surface decontamination by exposure to reactive oxygen species, methods of atomic or ionic oxygen generation differ. These differences may lead to unexpected results if the decontamination method is changed. Effects of UV-Ozone treatment and Corona treatments were compared to determine how a high-throughput Corona treatment could be substituted for UV-Ozone treatment. Due to inherently high cost and slow processing, oxygen plasma was not tested.

To quantify effect of UV-Ozone and Corona treatment on surface condition we measured the contact angle of a water droplet placed on the surface. This method is low-cost and non-destructive (see Appendix A). Figure 2a shows schematic of a water droplet and the measured contact angle. Figure 2b,c shows profile photos of water droplet before (after) 15 min UV-Ozone treatment on an ITO substrate. Initial testing indicated that 1000 Ws/m^2 dose of Corona treatment of an ITO film achieved water contact angle equivalent to 15 min UV-Ozone treatment.

When 1000 Ws/m^2 Corona treatment was substituted for UV-Ozone treatment of ITO film (before ZnO coating) no effect on film quality of device performance was observed and it was concluded that Corona treatment was a good substitute for UV-Ozone treatment.

Assuming the treatment rate was the same for ZnO as for the ITO surface, PbI_2 coating was tested on ZnO surfaces treated with 15 min UV-Ozone and 1000 Ws/m^2 Corona treatment. PbI_2 coated on ZnO films treated with UV-Ozone showed uniformly translucent texture, see Figure 2d,e. Unexpectedly, it was observed that ZnO films cleaned with Corona treatment frequently resulted in non-uniformly hazy texture of PbI_2 films, see Figure 2f,g.

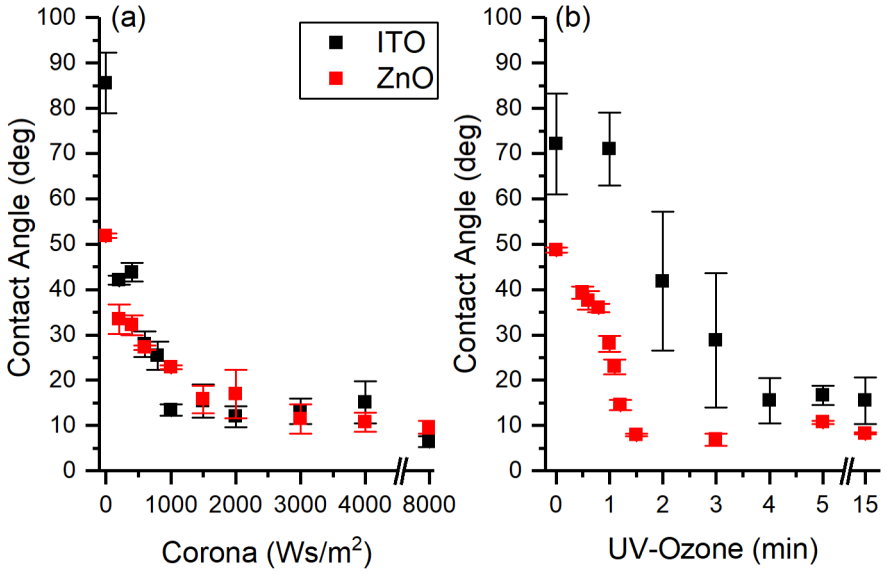

Figure 3.(a) Water contact angle dependence on corona treatment dose for ZnO (red squares) and ITO (black squares) surfaces. (b) Water contact angle dependence on UV-Ozone treatment time for ZnO (red squares) and ITO (black squares) surfaces. Error bars indicate standard deviation of three droplets measured for each treatment condition.

A detailed investigation of water contact angle dependence on UV-Ozone and Corona treatment dose was conducted. Figure 3a and b show the dependence of water drop contact angle on ITO and ZnO surfaces as a function of Corona and UV-Ozone treatment, respectively. The result indicated that water contact angle on ITO and ZnO depends very similarly on Corona treatment dose, however that is not true for UV-Ozone treatment. As seen in Figure 3b, UV-Ozone treatment decreases the water contact angle on ZnO dramatically faster than on an ITO surface. Although the water contact angle on a ZnO surface after 1000 Ws/m^2 Corona treatment is close to the contact angle achieved by 15 min UV-Ozone treatment, the texture of PbI_2 coated over Corona treated ZnO showed significant differences. UV-Ozone treatment achieves saturation (minimum measurable contact angle) after just 2 minutes on ZnO and around 1500 Ws/m^2 for Corona treatment. This observation suggests that some contamination may remain on the surface that cannot be detected by water contact angle measurements, but is removed by additional oxygen treatment.

To characterize surface contamination state, an XPS measurement was employed to quantitatively measure presence of carbon compounds on the sample surface. Figure 4 shows C 1s and O 1s XPS signals (normalized with respect to the Zn $2p_{3/2}$ peak height at the binding energy of 1022.5 eV) for ZnO surfaces treated with UV-Ozone and Corona. The raw XPS spectra were fitted with Gaussian-Lorentzian function in CASA XPS 2.3.16 software. Curve-fittings of XPS C 1s and O 1s core-level spectra were performed following procedure described in previous publication [16]. In Zn 2p core-level region (not shown), only a single

oxidation state with full width at half maximum (FWHM) of 1.7 eV in Zn $2p_{3/2}$ peak was measured and most likely associated with ZnO, ZnO_x, ZnOH, and/or C-Zn-O in agreement with previous reports[16, 18-21]. The C 1s core-level region exhibited three main chemical states at 285.5 eV, 287.3 eV and 289.5 eV (Figure 4a and c, marked 1,2,3 respectively)[16, 18-21]. As described in previous works, [16, 18-20] precise assignments of these carbon peaks are complex and an independent investigation will be required to correctly assign the chemical states in C 1s. Following literature, we tentatively assign the peak at 285.5 eV to adventitious carbon present at surface and bulk, 287.3 eV peak to surface contaminations related to O-C-O complexes (e.g. storage in air) [16, 18-20], and 289.5 eV peak to incorporated oxygen atoms at the interstitial sites of ZnO forming O-C-Zn complexes [16, 18] and/or shake-up line [22-25].

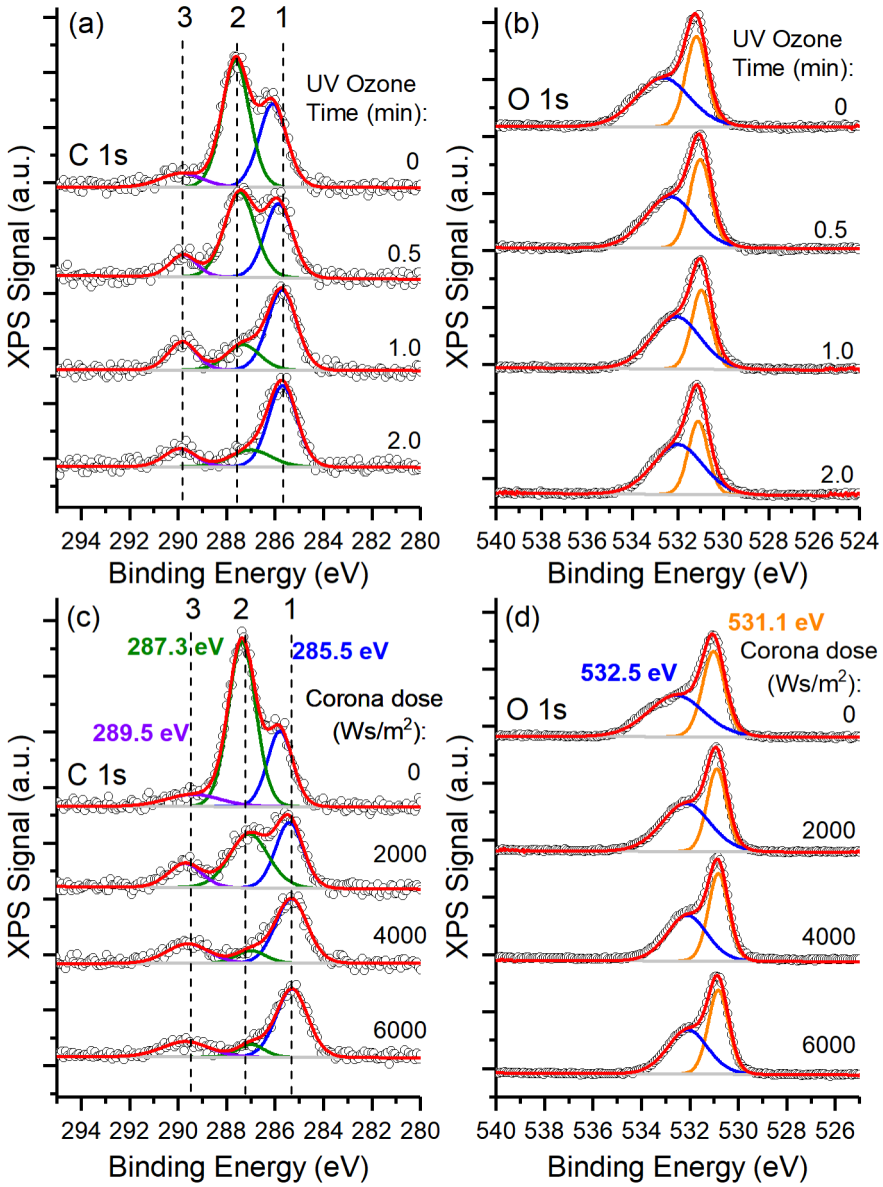

Figure 4 XPS signal of (a) C 1s and (b) O 1s after varying UV-Ozone treatment. XPS signal of (c) C 1s and (d) O 1s after varying Corona treatment. All XPS data were normalized to Zn 2p peak at 1022.5 eV. Plots in (a),(b), (c), and (d) are offset for clarity.

In this study, we focused on the systematic trend changes in the C 1s features that were correlated with slot-die coated PbI_2 film quality. It is observed that both types of treatment result in rapid decrease of C 1s signal at the binding energy of 287.3 eV (peak 2 in Figure 4a and c). Figure 5 summarizes dependence of C 1s peaks on UV Ozone and Corona treatment. It is observed that in agreement with water contact angle measurement, the 287.3 eV signal reaches a minimum value for UV-Ozone treatment after 2 minutes. For Corona treatment, after a dose of 2000 Ws/m^2 a substantial signal is still remaining at the binding energy of 287.3 eV. 4000 Ws/m^2 dose reaches the minimum C 1s signal value at the binding energy of 287.3 eV. In contrast, water contact angle measurements show no changes after Corona dose of 1500 Ws/m^2, see Figure 3a. In addition, it was considered that oxidation of the surface could lead to increased surface energy. The O 1s XPS signal is shown in Figure 4b and d. Similar to the C 1s region, XPS deconvolution in O 1s region is complex and further systematic studies will be required to assign correctly the chemical compounds (e.g. corroborated by FT-IR) present in our ZnO films. Comparing with literature reports[16, 18-20], the O 1s region is often deconvoluted in (i) stoichiometric ZnO lattice (~531.1 eV) and (ii) defective ZnO_x and/or hydroxyl complex of ZnOH (532.5 eV). However, because carbon-related contaminants are expected to contain oxygen atoms, our O 1s region is also expected to include these contaminants making the deconvolution of O 1s challenging. Because the O 1s peaks affected only slightly by Corona or UV-Ozone treatment, we conclude that surface energy increase is primarily due to organic (carbon containing) impurity removal.

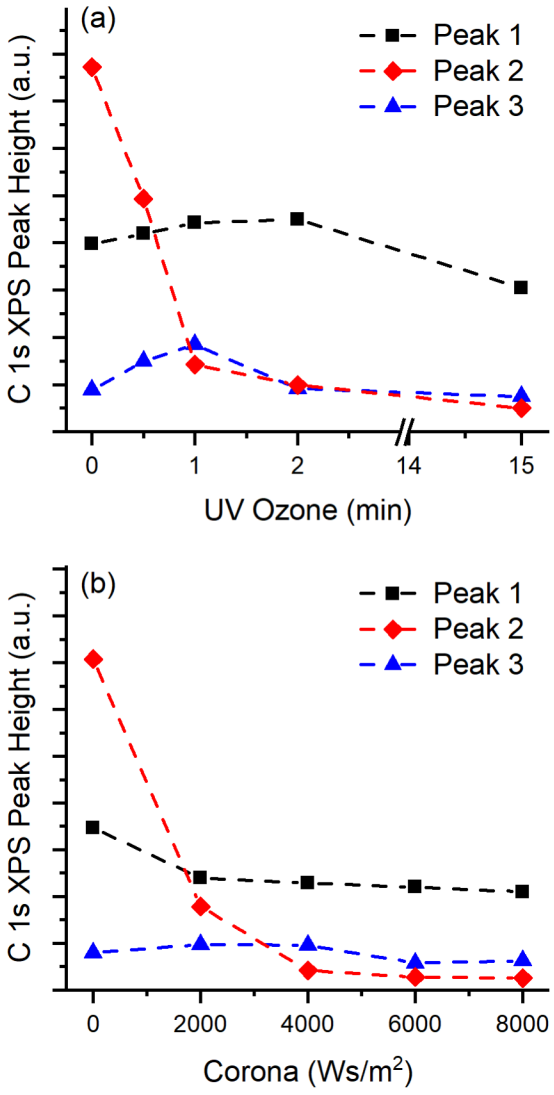

Figure 5 XPS signal of C 1s varying with (a) UV ozone and (b) Corona treatments. Peak positions of 1, 2, and 3 are marked in Figure 4.

182

183

184 Based on the observation that C 1s 287.3 eV XPS signal was undetectable after 4000 Ws/m^2 dose of Corona
185 treatment, PbI_2 coating process was tested with this Corona treatment dose. With the Corona treatment
186 done increased to 4000 Ws/m^2 visually observed PbI_2 film quality became equivalent to what was
187 observed for UV-Ozone treatment (Figure 2d-g). It was concluded that vanishing of the C 1s 287.3 XPS
188 signal was an indication of sufficient surface decontamination, and Corona treatment was good substitute
189 for UV-Ozone treatment. Due to many factors affecting the quality of solution processed devices
190 fabricated in ambient air, it is not straightforward to quantify the effect of a surface treatment on device
191 performance. To confirm our conclusion that increased Corona treatment dose improved film uniformity
192 and reproducibility we analyzed performance data of batches fabricated before and after it was
193 understood that that PbI_2 texture was affected by insufficient Corona treatment dose. Figure 6 shows

averaged PCE values for a series of device batches fabricated over a period of 3 months. A substantial increase in mean PCE and a reduction of standard deviation of device performance is observed after increased Corona treatment dose is implemented.

To understand the reason why a UV-Ozone, but not Corona treatment shows improved effectiveness on ZnO surface, we can consider the differences between two processes. Both processes generate atomic oxygen, but UV-Ozone also includes exposure to high energy UV radiation, while Corona does not. Both ITO and ZnO are high band-gap (ITO approx. 4 eV, ZnO approx. 3.3 eV) n-type semiconductors, and both are capable of absorbing the UV-light of UV-Ozone treatment (245 nm ~ 4.88 eV, 185 nm ~ 6.70 eV). However, ZnO is also known to be an efficient photocatalyst, with applications to pollutant decomposition [26]. An example of a photo-catalyzed reaction that could take place in presence of air and ZnO is reduction of molecular oxygen:

$$e^- + O_2 \rightarrow O_2^-$$

Superoxide (O_2^-) is a very reactive species that would be generated on the ZnO surface and accelerate decomposition of organic contaminants. Possible observation of photocatalytically assisted UV-Ozone decontamination suggests that a high-throughput UV-Ozone process could also be developed for selected surfaces. Furthermore, it is possible to develop a selective treatment process that would affect only photocatalytically active surfaces with minimal effect on other areas. This could be advantageous when the sample includes organic materials that could be damaged by extended oxygen treatment.

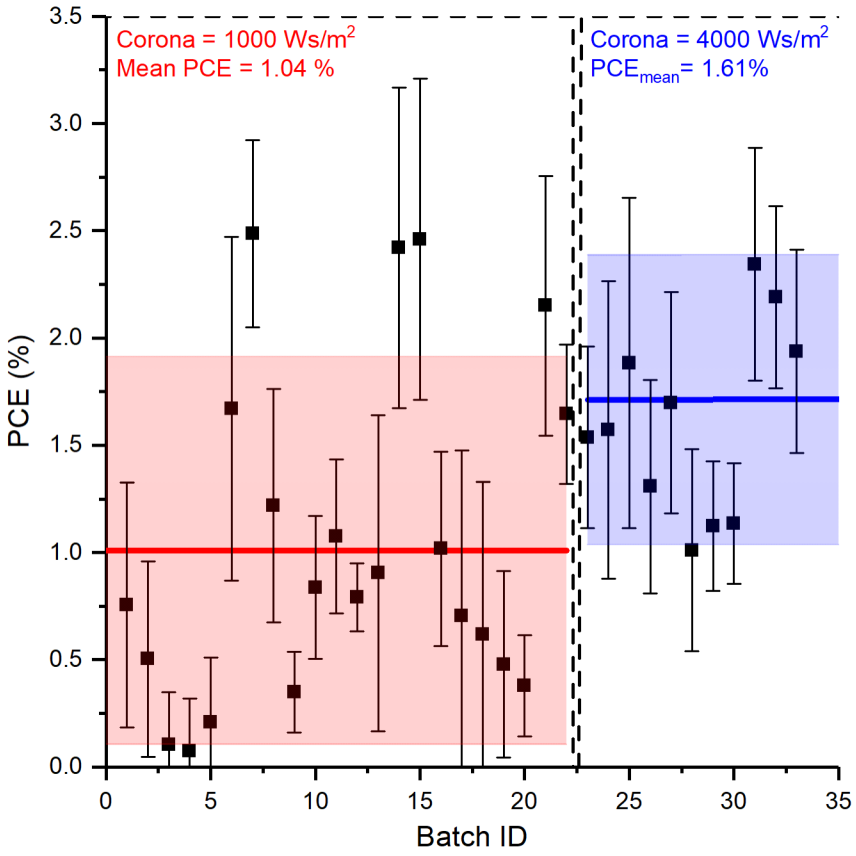

Figure 6. Performance data of slot-die coated samples fabricated over a time period of three months. Each data point represents a batch of 15 devices, of active area 1 cm^2, structure is illustrated in Figure 1c and e. Error bars are standard deviations. PCE is calculated by averaging forward and reverse IV measurements. Red solid line indicates mean PCE for samples treated with Corona dose based on ITO water contact angle measurement (1000 Ws/m^2). Blue solid line indicates mean PCE for samples treated with Corona dose based on XPS surface carbon measurement on ZnO surface (4000 Ws/m^2). Filled area indicates standard deviation. Batches are presented in chronological order of fabrication.

4 Conclusions

Key result of this study is that while water contact angle is a good guide to a degree of de-contamination achieved by different methods, trace contamination unresolvable through water contact angle may strongly affect uniformity of solution coated perovskite precursors. XPS carbon atomic density measurement provides a quantitative tool with the right sensitivity to identify full de-contamination of the surface. Water contact angle measurement followed by XPS measurement close to the optimal dose, is a cost-effective technique of determining correct oxygen treatment dose.

XPS measurement of carbon and oxygen density on ZnO surface suggests that the primary effect of Corona and UV-Ozone treatments is to remove carbon-containing contaminants rather than oxidize the surface. This is likely because ZnO is already an oxide, but may not be true for other types of surfaces.

We have successfully demonstrated that UV-ozone treatment could be substituted with high-throughput Corona treatment in a slot-die coating process for a perovskite solar cell. Equivalent PbI_2 film quality was

achieved with treatment time (for a 10 x 10 cm substrate) reduced from 15 min (UV-Ozone) to 0.1 s (Corona).

It is observed that decontamination of ZnO surface by UV-Ozone is greatly accelerated, compared to ITO surface. This effect is not observed for Corona treatment. A possible explanation for this effect is photocatalytic production of O_2^- (superoxide ion) on the surface of ZnO due to UV light exposure. Presence of superoxide ion would accelerate decomposition of surface adsorbed organic species. Rapid decontamination of ZnO by UV-Ozone suggests that even UV-Ozone may be useful in high-throughput production. In particular, if delicate polymer substrates are employed, UV-Ozone could be employed to selectively treat ZnO coated areas, with reduced risk of damage to the polymer substrate.

5 Acknowledgements

This work was supported by funding from the Energy Materials and Surface Sciences Unit of the Okinawa Institute of Science and Technology Graduate University, the OIST R&D Cluster Research Program, and the OIST Proof of Concept (POC) Program.

Appendix A. Surface energy

The surface treatments discussed in this article are primarily aimed at de-contamination of surfaces and increasing the surface energy, therefore the concept of surface energy is briefly discussed. Surface energy is defined as the energy required to change the surface area of an object by a unit of area. The concept originates from the fact that surface atoms are not uniformly surrounded by identical atoms (unlike the atoms inside the solid or liquid) and therefore exist in a higher energy state. An alternative term "surface tension" is also frequently used to refer to surface energy of liquids. The terms refer to the same quantity and the common surface tension units of dyn/cm are equivalent to surface energy unit of mJ/cm^2. For a liquid, surface energy can be determined directly by measuring energy required to stretch a fixed liquid volume, therefore increasing its surface area. For a solid, deformation would involve many other energy-consuming processes, therefore literal implementation of the definition is not practical.

Many methods of measuring solid surface energy exist, but two simple methods are most common in non-specialized laboratory settings: water contact angle and dyne liquids [27]. Dyne liquids are special mixtures of known surface tension available in increments of 10 dyn/cm. Drawing a line on the surface of a solid by a specified dyne liquid pen will result in a line that is either continuous or breaks into beads. A continuous line indicates that solid has higher surface energy than the dyne liquid and vice versa.

The water contact angle method means placing a small drop of water on the surface and using a camera to photograph the water drop profile. The contact angle of the water to the solid surface will depend on the surface energy of the solid. In a highly idealized case of a pure water droplet on a perfectly clean solid surface, contact angle can be related to surface energy via Young equation:

$$\gamma_{SG} = \gamma_{SL} + \gamma_{LG} \cos\theta$$

Where γ_{SG} is surface energy of the solid-gas interface, γ_{SL} is surface energy of the solid-liquid interface, and γ_{LG} is surface energy of the liquid-gas interface (see Figure 2a). Differences between the three surface energies act like forces to displace the edge of the liquid drop and equilibrium is achieved when all three

exactly cancel. In a practical measurement, droplet edge will generally be pinned to some extent, and the measured contact angle will depend on whether the liquid edge was advancing or receding before stabilizing (see Figure 2a). The true equilibrium angle is between advancing and receding values, but cannot be determined by any simple method. In practice, however, to compare surface energies of surfaces, identical droplet placement will ensure that contact angle difference will reflect difference in surface energy.

Equilibrium contact angle between liquid ink and the substrate is a crucial parameter that determines the uniformity of coating. A high contact angle will result in dewetting of ink rather than uniform coverage of the substrate. Even when complete coverage is achieved, a high contact angle may lead to slow equilibration of ink into a flat wet film. Slow equilibration may result in precipitation of ink solids before a flat wet film is achieved, which is highly detrimental to coating uniformity. Therefore, various surface treatments are applied to maximize surface energy and ensure rapid wet film equilibration. It is worth noting that while contact angle measurements are typically performed with water droplets, the obtained estimate of surface energy is applicable to coating with any solvent. Most organic solvents have low surface tension (< 40 dyn/cm) while water has high surface tension (74 dyn/cm) resulting in a higher contact angle and higher precision of measurement. However, even with a low surface tension solvent, maximizing substrate surface energy is desirable for rapid equilibration of ink coating.

Appendix B. Types of surface treatment

Three dry surface cleaning methods are popular in typical semiconductor process laboratories: UV-Ozone, Oxygen plasma, and Corona discharge. All three methods accomplish the goal of removing contaminants from the surface and partially oxidizing the surface. Both de-contamination and oxidation act to increase surface energy and are not distinguishable by liquid contact angle measurements. However, formation of oxide layer could impact charge carrier transport through the interface between functional layers and affect device performance.

UV-Ozone treatment is accomplished by placing the sample in an enclosed chamber illuminated by a UV light. A typical apparatus uses the mercury discharge light which emits UV light at wavelengths of 185 nm and 254 nm. 185nm light is absorbed by oxygen present in air (while 254 nm is not) and causes formation of atomic oxygen and ozone [28]:

$O_2 + h\nu\ (< 242\text{nm}) \rightarrow O + O$

$O + O_2 + M \rightarrow O_3 + M$

Where M is any neutral molecule that is necessary to conserve momentum. Ozone strongly absorbs UV light (including the 254 nm light) and decomposes via reaction

$O_3 + h\nu\ (< 1200\ \text{nm}) \rightarrow O_2 + O$

The highly reactive atomic oxygen will oxidize surface molecules of the sample and adsorbed contaminants. Organic molecules that decompose into volatile species under oxidation will leave the surface, and the sample is effectively cleaned. Oxygen will also react with sample surface to form oxide and hydroxide groups which have higher surface energy, increasing the wettability of the surface.

UV light that is not absorbed by air may be absorbed by the surface and also cause decomposition of surface contaminants. It was observed in [17] that exposure to either UV light (wavelength > 242 nm, with

insufficient photon energy to generate ozone) or ozone caused the surface cleaning to occur at a slow rate, whereas exposure to both resulted in contamination removal about 100 times faster. Observation was interpreted to mean that exposure to UV light greatly increases reactivity of surface contaminants and atomic oxygen.

UV-Ozone cleaning is popular due to its simple operation and low maintenance. The rate of treatment depends on the distance to the UV lamp, but sample height variations on the order of centimeters can be accommodated in a typical laboratory setup.

Corona discharge treatment is accomplished by passing a sample surface close to an arc discharge between two high-voltage electrodes in air. Alternating high voltage between the electrodes accelerates naturally occurring free charges, causing high energy collisions and further ionization of the air. The discharge results in a high concentration of atomic oxygen which oxidizes contaminants on the surface. Oxidized organic molecules that form volatile species are removed. Surface of the sample is also oxidized introducing oxide and hydroxide groups, which have high surface energy and increase wettability of the surface [29]. Ozone is also generated in the process, but in absence of UV-illumination it does not play a significant role in the surface treatment. Instead, Ozone generation needs to be considered from the safety perspective to ensure that this toxic gas is channeled to appropriate exhaust.

The absence of UV illumination in the process means that the treatment is confined strictly to the surface of the sample and there is no risk of UV radiation penetrating and damaging the substrate. Generally Corona treatment is applied to flat surfaces or continuous films, because a uniform treatment requires uniform distance (with sub-millimeter accuracy) between the sample and the electrode. Variations of Corona treatment tools exist that channel the plasma using a flow of air making it possible to treat non-flat surfaces. However, the majority of the plasma is still confined to the vicinity of electrodes making this process much less energy efficient [29].

Oxygen plasma treatment is accomplished by placing a sample in a sealed chamber filled with oxygen at a low pressure between 1000 mTorr and 10 mTorr. An alternating electric field (frequency in the KHz – MHz range) is applied to accelerate naturally occurring ions, which causes further ionization, until a large fraction of the gas becomes ionized. Resulting atmosphere of ionized atomic oxygen in extremely reactive and will rapidly oxidize any un-oxidized species. Organic and other carbon-containing compounds will typically form volatile species and be removed from the chamber by the vacuum system.

The plasma treatment is the most powerful of the three methods described in this work. It is the only method that is capable of rapidly removing bulk quantities of organic materials. For that reason it is not suitable for treating substrates containing functional organic materials deposited intentionally. Any organic components exposed to the plasma will be damaged or completely removed.

References

[1] (2017-06-26). *NREL Efficiency Chart*. Available: http://www.nrel.gov/ncpv/images/efficiency_chart.jpg

[2] Z. Gu *et al.*, "Interfacial engineering of self-assembled monolayer modified semi-roll-to-roll planar heterojunction perovskite solar cells on flexible substrates," *J. Mater. Chem. A,* vol. 3, no. 48, pp. 24254-24260, 2015.

[3] K. Hwang *et al.*, "Toward Large Scale Roll-to-Roll Production of Fully Printed Perovskite Solar Cells," *Advanced Materials,* vol. 27, no. 7, pp. 1241-1247, 2015.
[4] T. M. Schmidt, T. T. Larsen-Olsen, J. E. Carlé, D. Angmo, and F. C. Krebs, "Upscaling of Perovskite Solar Cells: Fully Ambient Roll Processing of Flexible Perovskite Solar Cells with Printed Back Electrodes," *Advanced Energy Materials,* vol. 5, no. 15, p. 1500569, 2015.
[5] G. Cotella *et al.*, "One-step deposition by slot-die coating of mixed lead halide perovskite for photovoltaic applications," *Solar Energy Materials and Solar Cells,* vol. 159, pp. 362-369, 2017.
[6] T. Qin *et al.*, "Amorphous hole-transporting layer in slot-die coated perovskite solar cells," *Nano Energy,* vol. 31, pp. 210-217, 2017.
[7] J. Ciro, M. A. Mejía-Escobar, and F. Jaramillo, "Slot-die processing of flexible perovskite solar cells in ambient conditions," *Solar Energy,* vol. 150, pp. 570-576, 2017.
[8] D. Vak *et al.*, "3D Printer Based Slot-Die Coater as a Lab-to-Fab Translation Tool for Solution-Processed Solar Cells," *Advanced Energy Materials,* vol. 5, no. 4, p. 1401539, 2015.
[9] W.-C. Chang, D.-H. Lan, K.-M. Lee, X.-F. Wang, and C.-L. Liu, "Controlled Deposition and Performance Optimization of Perovskite Solar Cells Using Ultrasonic Spray-Coating of Photoactive Layers," *ChemSusChem,* vol. 10, no. 7, pp. 1405-1412, 2017.
[10] A. T. Barrows, A. J. Pearson, C. K. Kwak, A. D. F. Dunbar, A. R. Buckley, and D. G. Lidzey, "Efficient planar heterojunction mixed-halide perovskite solar cells deposited via spray-deposition," *Energy & Environmental Science,* vol. 7, no. 9, p. 2944, 2014.
[11] S. Das *et al.*, "High-Performance Flexible Perovskite Solar Cells by Using a Combination of Ultrasonic Spray-Coating and Low Thermal Budget Photonic Curing," *ACS Photonics,* vol. 2, no. 6, pp. 680-686, 2015.
[12] J. G. Tait *et al.*, "Rapid composition screening for perovskite photovoltaics via concurrently pumped ultrasonic spray coating," *J. Mater. Chem. A,* vol. 4, no. 10, pp. 3792-3797, 2016.
[13] D. K. Mohamad, J. Griffin, C. Bracher, A. T. Barrows, and D. G. Lidzey, "Spray-Cast Multilayer Organometal Perovskite Solar Cells Fabricated in Air," *Advanced Energy Materials,* vol. 6, no. 22, p. 1600994, 2016.
[14] H. Huang, J. Shi, L. Zhu, D. Li, Y. Luo, and Q. Meng, "Two-step ultrasonic spray deposition of CH 3 NH 3 PbI 3 for efficient and large-area perovskite solar cell," *Nano Energy,* vol. 27, pp. 352-358, 2016.
[15] M. Remeika, S. R. Raga, S. Zhang, and Y. B. Qi, "Transferrable optimization of spray-coated PbI2 films for perovskite solar cell fabrication," *J. Mater. Chem. A,* vol. 5, no. 12, pp. 5709-5718, 2017.
[16] Y. Kato, M.-C. Jung, M. V. Lee, and Y. B. Qi, "Electrical and optical properties of transparent flexible electrodes: Effects of UV ozone and oxygen plasma treatments," *Organic Electronics,* vol. 15, no. 3, pp. 721-728, 2014.
[17] J. Vig and J. LeBus, "UV/Ozone Cleaning of Surfaces," *IEEE Transactions on Parts, Hybrids, and Packaging,* vol. 12, no. 4, pp. 365-370, 1976.
[18] S. T. Tan, X. W. Sun, Z. G. Yu, P. Wu, G. Q. Lo, and D. L. Kwong, "p-type conduction in unintentional carbon-doped ZnO thin films," *Applied Physics Letters,* vol. 91, no. 7, 2007.
[19] Y. Du *et al.*, "Improvement of bond strength between ZnO nanorods and carbon fibers using magnetron sputtered ZnO films as the interphase," *CrystEngComm,* vol. 19, no. 5, pp. 868-875, 2017.
[20] O. Lupan *et al.*, "Synthesis and Characterization of Ag- or Sb-Doped ZnO Nanorods by a Facile Hydrothermal Route," *The Journal of Physical Chemistry C,* vol. 114, no. 29, pp. 12401-12408, 2010.
[21] M. C. Biesinger, L. W. M. Lau, A. R. Gerson, and R. S. C. Smart, "Resolving surface chemical states in XPS analysis of first row transition metals, oxides and hydroxides: Sc, Ti, V, Cu and Zn," *Applied Surface Science,* vol. 257, no. 3, pp. 887-898, 2010.

[22] W. M. R. C.D. Wagner, L.E. Davis, J.F. Moulder, G.E. Muilenberg, *Handbook of X-ray Photoelectron Spectroscopy*. Minnesota: Perkin-Elmer Corp, 1979.

[23] G. Patrinoiu *et al.*, "Sustainable one-pot integration of ZnO nanoparticles into carbon spheres: manipulation of the morphological, optical and electrochemical properties," *Phys. Chem. Chem. Phys.,* vol. 18, no. 44, pp. 30794-30807, 2016.

[24] M. Smith, L. Scudiero, J. Espinal, J.-S. McEwen, and M. Garcia-Perez, "Improving the deconvolution and interpretation of XPS spectra from chars by ab initio calculations," *Carbon,* vol. 110, pp. 155-171, 2016.

[25] D. Benne, E. Maccallini, P. Rudolf, C. Sooambar, and M. Prato, "X-ray photoemission spectroscopy study on the effects of functionalization in fulleropyrrolidine and pyrrolidine derivatives," *Carbon,* vol. 44, no. 14, pp. 2896-2903, 2006.

[26] K. M. Lee, C. W. Lai, K. S. Ngai, and J. C. Juan, "Recent developments of zinc oxide based photocatalyst in water treatment technology: A review," *Water Research,* vol. 88, pp. 428-448, 2016.

[27] A. Kuhn, "Starting off with a clean slate," *Metal Finishing,* vol. 103, no. 5, pp. 72-79, 2005.

[28] P. Fabian, *Ozone in the atmosphere*. New York: Springer, 2014, p. pages cm.

[29] S. Ebnesajjad and C. F. Ebnesajjad, *Surface treatment of materials for adhesive bonding*, Second edition. ed. Amsterdam: William Andrew, an imprint of Elsevier, 2014, pp. xvii, 341 pages.